The Astrophysical Journal, 774:78 (13pp), 2013 September 1 doi:10.1088/0004-637X/774/1/78

THE INFLUENCE OF INELASTIC NEUTRINO REACTIONS WITH LIGHT NUCLEI ON THE STANDING ACCRETION SHOCK INSTABILITY IN CORE-COLLAPSE SUPERNOVAE

Shun Furusawa[1], Hiroki Nagakura[1,2], Kohsuke Sumiyoshi[3], and Shoichi Yamada[1,4]
[1] Advanced Research Institute for Science and Engineering, Waseda University, 3-4-1, Okubo, Shinjuku, Tokyo 169-8555, Japan; furusawa@heap.phys.waseda.ac.jp
[2] Yukawa Institute for Theoretical Physics, Kyoto University, Oiwake-cho, Kitashirakawa, Sakyo-ku, Kyoto 606-8502, Japan
[3] Numazu College of Technology, Ooka 3600, Numazu, Shizuoka 410-8501, Japan
[4] Department of Science and Engineering, Waseda University, 3-4-1 Okubo, Shinjuku, Tokyo 169-8555, Japan
Received 2013 April 10; accepted 2013 July 5; published 2013 August 19

ABSTRACT

We perform numerical experiments to investigate the influence of inelastic neutrino reactions with light nuclei on the standing accretion shock instability (SASI). The time evolution of shock waves is calculated with a simple light-bulb approximation for the neutrino transport and a multi-nuclei equation of state. The neutrino absorptions and inelastic interactions with deuterons, tritons, helions, and alpha particles are taken into account in the hydrodynamical simulations. In addition, the effects of ordinary charged-current interactions with nucleons is addressed in the simulations. Axial symmetry is assumed but no equatorial symmetry is imposed. We show that the heating rates of deuterons reach as high as ∼10% of those of nucleons around the bottom of the gain region. On the other hand, alpha particles are heated near the shock wave, which is important when the shock wave expands and the density and temperature of matter become low. It is also found that the models with heating by light nuclei evolve differently in the non-linear phase of SASI than do models that lack heating by light nuclei. This result is because matter in the gain region has a varying density and temperature and therefore sub-regions appear that are locally rich in deuterons and alpha particles. Although the light nuclei are never dominant heating sources and they work favorably for shock revival in some cases and unfavorably in other cases, they are non-negligible and warrant further investigation.

Key words: equation of state – hydrodynamics – neutrinos – supernovae: general

Online-only material: color figures

1. INTRODUCTION

The mechanism of core-collapse supernovae is not clearly understood at present because of its detailed nature (see, e.g., Kotake et al. 2006; Janka 2012; Burrows 2013). Many numerical simulations performed by different groups have consistently demonstrated that the shock waves formed by the bounce of collapsing cores are decelerated and stalled by the energy losses due to the dissociations of nuclei and the emission of neutrinos. For the moment, neutrino heating is thought to be the most promising mechanism for shock revival, in which the neutrinos emitted from the proto-neutron star reinvigorate the stalled shock and cause it to propagate outward again. However, some other mechanisms, e.g., magneto-rotational explosions, may be needed for very massive stars. It is also believed that the so-called standing accretion shock instability (SASI) and convection are essential for increasing the efficiency of neutrino heating (Herant et al. 1992; Burrows et al. 1995; Fryer et al. 2002; Blondin et al. 2003; Fryer 2004; Scheck et al. 2004, 2006; Ohnishi et al. 2006; Foglizzo et al. 2006, 2007, 2012; Iwakami et al. 2008, 2009; Fernández & Thompson 2009a, 2009b; Fernández 2010; Hanke et al. 2012, 2013; Müller et al. 2012; Bruenn et al. 2013; Ott et al. 2013; Murphy et al. 2013). Indeed, recent multi-dimensional numerical simulations have successfully relaunched the stalled shock wave; these simulations may eventually produce supernova explosions as we see them (Buras et al. 2006a, 2006b; Marek & Janka 2009; Suwa et al. 2010, 2011; Müller et al. 2012; Kuroda et al. 2012; Takiwaki et al. 2012; Bruenn et al. 2013; Ott et al. 2013; Murphy et al. 2013). All of these simulations do not extend for enough in the time domain, however, and it remains to be see if they can truly reproduce the canonical explosion energy and the ^{56}Ni mass (Yamamoto et al. 2013). In addition to these hydrodynamical effects, there are several nuclear-physical ingredients that are also supposed to be important for reproducing the core-collapse supernovae. Nuclear burning in the accreting matter and ejecta was investigated by Nakamura et al. (2013) and Yamamoto et al. (2013). The inelastic neutrino interactions, as well as the baryonic equation of state (EOS), are also important, as described below.

The inelastic interactions between neutrinos and nuclei have been neglected in most hydrodynamical simulations of the neutrino heating. Haxton (1988) was the first to point out the importance of these reactions. O'Connor et al. (2007), Arcones et al. (2008), Langanke et al. (2008), and Barnea et al. (2008) investigated the influence of inelastic interactions on dynamics, the neutrino spectrum, and nucleosynthesis. However, there have been no investigations of the impact of the inelastic reactions on multi-dimensional hydrodynamics except for that of Ohnishi et al. (2007). These authors showed that the inelastic neutrino interactions with alpha particles are helpful in reviving the shock in two-dimensional (2D) simulations if the neutrino luminosity is close to the critical value (the threshold for shock revival). Ohnishi et al. (2007) took into account only alpha particles as additional heating sources, since the mass fractions of other nuclei were not available in the EOS that they used (Shen et al. 1998a, 1998b). However, the shocked matter is certainly composed not only of nucleons and alpha particles but also of deuterons, tritons, and helions (Sumiyoshi & Röpke 2008; Arcones et al. 2008; Hempel et al. 2012). The energy-transfer coefficients, that is, the average values of the product of the cross section and energy transfer of deuterons, are comparable to those of nucleons and ten times greater than those of alpha particles (Nakamura et al. 2009). Tritons and helions have also larger

energy-transfer coefficients than alpha particles (O'Connor et al. 2007; Arcones et al. 2008; Nakamura et al. 2009).

The EOS is another important physical input in supernova simulations and its influence on the dynamics of core-collapse supernovae has been investigated by many researchers, e.g., Sumiyoshi et al. (2005), Marek et al. (2009), Hempel et al. (2012), Suwa et al. (2013), and Couch (2013), to mention a few. There are currently two EOSs that are widely used for simulations: Lattimer–Swesty's EOS (Lattimer et al. 1991) and Shen's EOS (Shen et al. 1998a, 1998b, 2011b). In both EOSs, the ensemble of heavy and light nuclei is approximated by a single representative heavy nucleus and alpha particle. In the past decade, however, some EOSs that incorporate a large number of nuclei have been constructed (Botvian et al. 2004; Botvina et al. 2010; Hempel et al. 2010; Blinnikov et al. 2011; Shen et al. 2011a). We have also developed such an EOS (Furusawa et al. 2011, 2013). We employed the liquid drop model for heavy nuclei and took into account shell effects and nuclear pasta phases. Unbound nucleons were treated by the relativistic mean field theory (Furusawa et al. 2011). Moreover, we implemented some important improvements such as the inclusion of the Pauli and self-energy shifts in the mass evaluation of light nuclei (Furusawa et al. 2013). As a result, the mass fractions of various light nuclei have become much more reliable.

The aim of this paper is to investigate the impacts of the inelastic neutrino reactions with light nuclei on the SASI based on our new EOS. We perform experimental simulations of the post-bounce phase in 2D, employing the light bulb approximation for neutrino transfer. In addition to the ordinary cooling and heating by nucleons, we incorporate heating by deuterons, tritons, helions, and alpha particles. This paper is organized as follows. In Section 2, we describe some important ingredients in numerical simulations such as the hydrodynamics code and the rates of inelastic reactions with light nuclei that we employ in this study. Then, the results are shown in Section 3, with an emphasis put on the role of light nuclei in the shock heating. The paper is concluded with a summary and some discussions in Section 4.

2. MODELS

The basic set-up of our dynamical simulations is the same as that given in Ohnishi et al. (2006, 2007) and Nagakura et al. (2013), except for an inelastic reactions with light nuclei. We perform 2D simulations assuming axial symmetry. Spherical coordinates are used and no equatorial symmetry is assumed. We utilized 300 radial mesh points to cover $r_{\rm in} \leqslant r \leqslant r_{\rm out}$ (=500 km), where $r_{\rm in}$, the inner boundary of the computation domain, is set to be the radius of the neutrino sphere of ν_e in the initial state. We used 60 angular mesh points to cover the whole meridian section. We solved the following equations:

$$\frac{d\rho}{dt} + \rho\nabla\cdot \mathrm{v} = 0, \tag{1}$$

$$\rho\frac{d\mathrm{v}}{dt} = -\nabla p + \rho\nabla\left(\frac{GM_{\rm in}}{r}\right), \tag{2}$$

$$\rho\frac{d}{dt}\left(\frac{e}{\rho}\right) = -p\nabla\cdot\mathrm{v} + Q_E + Q_d + Q_t + Q_h + Q_\alpha, \tag{3}$$

$$\frac{dY_e}{dt} = Q_N, \tag{4}$$

where ρ, p, T, e, and Y_e denote the mass density, pressure, temperature, energy density, and electron fraction, respectively. Other symbols, r, v, and G, stand for the radius, fluid velocity, and the gravitational constant, respectively. The mass of a central object, $M_{\rm in}$, is assumed to be constant and is set to be $M_{\rm in} = 1.4\,M_\odot$. Interactions between neutrinos and nucleons are encapsulated in Q_E and Q_N, the expressions of which are adopted from Equations (16) and (17) in Ohnishi et al. (2006). $Q_{d,t,h,\alpha}$ are the heating rates for the light nuclei indicated by the subscripts. The heating for alpha particles, Q_α, corresponds to $Q_{\rm inel}$ in Equations (3) and (6) in Ohnishi et al. (2007), where only alpha particles were taken into account as the additional heating source. The heating rates for deuterons, tritons and helions, $Q_{d,t,h}$, are the new elements in this work.

The neutrino transport is handled by the simple light bulb approximation, in which neutrinos with Fermi–Dirac distributions are assumed to be emitted from the proto-neutron star and travel radially. We also assume that the temperatures of $\nu_{\rm e}$, $\bar{\nu}_{\rm e}$, and ν_μ are constant and equal to $(T_{\nu_{\rm e}}, T_{\bar{\nu}_{\rm e}}, T_{\nu_\mu}) = (4, 5, 10)$ MeV. The luminosities of $\nu_{\rm e}$ and $\bar{\nu}_{\rm e}$ are assumed to have the same value: $L_{\nu_{\rm e}} = L_{\bar{\nu}_{\rm e}} = L$. The luminosity of ν_μ is set to be half that value, $L_{\nu_\mu} = 0.5 \times L$, as in Ohnishi et al. (2007). The numerical hydrodynamics code is based on the central scheme, which is a popular choice at the present time (see, e.g., Nagakura & Yamada 2008; Nagakura et al. 2011) and the implementation of the light bulb approximation is explained in detail in Nagakura et al. (2013). We employ the multi-nuclei EOS, which gives not only thermodynamical quantities but also the abundance of various light and heavy nuclei with mass numbers up to $A \sim 1000$ (Furusawa et al. 2011, 2013).

The heating rates for light nuclei are calculated from the analytic formula given in Haxton (1988):

$$\begin{aligned} Q_i = \frac{\rho X_i}{m_u}\frac{31.6\,\mathrm{MeV\,s^{-1}}}{(r/10^7\,\mathrm{cm})^2}\Bigg[&\frac{L_{\nu_{\rm e}}}{10^{52}\,\mathrm{erg\,s^{-1}}}\left(\frac{5\,\mathrm{MeV}}{T_{\nu_{\rm e}}}\right) \\ &\times \frac{A_i^{-1}\langle\sigma^+_{\nu_{\rm e}}E_{\nu_{\rm e}} + \sigma^0_{\nu_{\rm e}}E^i_{\rm NC}\rangle_{T_{\nu_{\rm e}}}}{10^{-40}\,\mathrm{cm^2\,MeV}} \\ &+ \frac{L_{\bar{\nu}_{\rm e}}}{10^{52}\,\mathrm{erg\,s^{-1}}}\left(\frac{5\,\mathrm{MeV}}{T_{\bar{\nu}_{\rm e}}}\right)\frac{A_i^{-1}\langle\sigma^-_{\bar{\nu}_{\rm e}}E_{\nu_{\rm e}} + \sigma^0_{\bar{\nu}_{\rm e}}E^i_{\rm NC}\rangle_{T_{\bar{\nu}_{\rm e}}}}{10^{-40}\,\mathrm{cm^2\,MeV}} \\ &+ \frac{L_{\nu_\mu}}{10^{52}\,\mathrm{erg\,s^{-1}}}\left(\frac{10\,\mathrm{MeV}}{T_{\nu_\mu}}\right)\frac{A_i^{-1}\langle\sigma^0_{\nu_\mu}E^i_{\rm NC} + \sigma^0_{\bar{\nu}_\mu}E^i_{\rm NC}\rangle_{T_{\nu_\mu}}}{10^{-40}\,\mathrm{cm^2\,MeV}}\Bigg], \end{aligned} \tag{5}$$

where i specifies a light nucleus, d, t, h or α; A_i and X_i are the mass number and mass fraction of the nucleus i, respectively; m_u is the atomic mass unit; and the average over the neutrino spectrum is denoted as $\langle\,\rangle_T$. The energy-transfer coefficients for deuterons are calculated from Table I in Nakamura et al. (2009) for both the neutral-current (NC), $\langle\sigma^0_\nu E^i_{\rm NC}\rangle_T$, and the charged-current (CC),$\langle\sigma^\pm_\nu E_\nu\rangle_T$. The energy-transfer coefficients for the nuclei with $A_i = 3$ (tritons and helions) are obtained from Table II in O'Connor et al. (2007) for the NC. We utilize values from Table I of Arcones et al. (2008) for the CC interactions between tritons and $\bar{\nu}_{\rm e}$. The other CC reactions involving tritons or helions are not included in our simulations, since neither the energy-transfer coefficients nor the cross sections are available. The effects of helions are negligible, however, since the abundance of helions is much smaller than nucleons and dominant light nuclei (deuterons of alpha particles). The energy-transfer coefficients for alpha particles are derived from

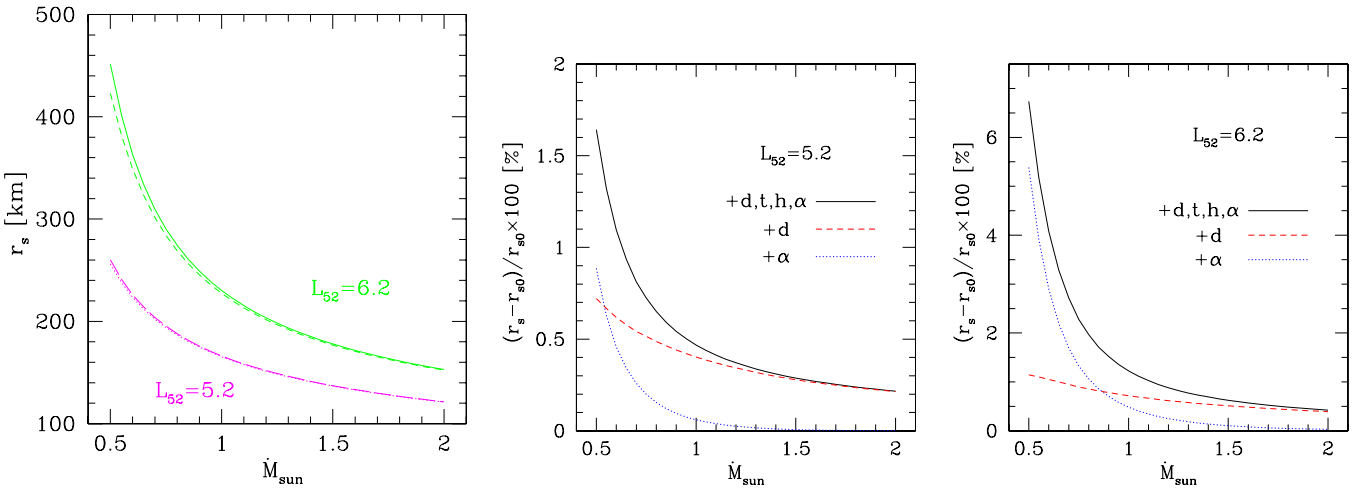

Figure 1. Left panel shows the shock radius vs. the mass accretion rate in the initial steady state for $L_{52} = 6.2$ with light-nuclei heating (green solid line) and without it (green dashed line). The case of $L_{52} = 5.2$ with light-nuclei heating (magenta long dashed line) and without it (magenta dotted line) is also shown. The center and right panels show the variations of shock radius due to the heating reactions with all light nuclei (black solid line), only deuterons (red dashed line), and only alpha particles (blue dotted line).

(A color version of this figure is available in the online journal.)

Table II in Haxton (1988) for the CC whereas we utilize the fitting formula provided by Haxton (1988) for the NC:

$$A_i^{-1}\langle\sigma_\nu^0 E_{\rm NC}^i + \sigma_{\bar\nu}^0 E_{\rm NC}^i\rangle_{T_\nu} = \alpha\left[\frac{T_\nu - T_0}{10\,{\rm MeV}}\right]^\beta, \quad (6)$$

where the parameters are chosen to be $\alpha = 1.28 \times 10^{-40}$ MeV cm^2, $\beta = 4.46$, and $T_0 = 2.05$ MeV following Gazit & Barnea (2004). The cooling reactions involving light nuclei are ignored, since the reaction rates are not available at the moment. In this sense, the influence of light nuclei that we find in this paper should be regarded as upper limits. We also ignore the contributions of charged-current interactions of light nuclei to the evolution of the electron fraction (Equation (4)), as in Ohnishi et al. (2007), since they are quite minor compared to the contributions of nucleons in most regions, as demonstrated at the end of the next section.

As the first step of the simulations, we prepare the initial conditions, which are spherically symmetric, steady accretion flows that are stable to radial perturbations (Yamasaki & Yamada 2005; Ohnishi et al. 2006; Nagakura et al. 2013). The inelastic interactions of neutrinos with light nuclei, $Q_{d,t,h,\alpha}$, are also included in these computations. We start dynamical simulations, adding radial-velocity perturbations of 1%, which are proportional to $\cos\theta$, where θ is the polar angle. We vary the luminosity L and mass accretion rate $\dot M$ and investigate the influence of the light nuclei on the dynamics under different physical conditions. We refer to the normalized neutrino luminosity $L_{52} \equiv L/(10^{52}\,{\rm erg\,s^{-1}})$ and the mass accretion rate $\dot M_{\rm sun} \equiv -\dot M/(M_\odot\,{\rm s^{-1}})$ when we specify models.

3. RESULT

In the following subsections, we first discuss the influence of the light nuclei on the initial states, that is, the spherically symmetric, steady accretion flows through the standing shock wave onto the proto-neutron star. Then, a one-dimensional (1D) simulation is presented to provide insight into the roles of the light nuclei. Finally, we describe the results of the 2D dynamical simulations in detail.

Table 1
The Heating Rates of Nucleons, Deuterons, Tritons, Helions, and Alpha Particles in Units of MeV s^{-1} per Baryon

Flavor	n, p	d	t	h	α
ν_e (CC)	356.8	168.9	0.000	0.000	0.5925
$\bar\nu_e$ (CC)	557.5	169.1	8.015	0.000	1.896
ν_e (NC)	0.000	12.94	0.6656	0.7446	0.008347
$\bar\nu_e$ (NC)	0.000	16.83	1.801	1.975	0.4231
ν_μ (NC)	0.000	139.0	31.05	32.55	17.61

Notes. $X_p = 0.5$ and $X_n = 0.5$ are assumed in the calculations for nucleons. The mass fraction of each light nucleus is set to unity in the calculation for light nuclei; $X_{d,h,t,\alpha} = 1$. Other parameters are set at $r = 100$ km, $L_{\nu_e,\bar\nu_e} = 5.0 \times 10^{52}$ erg s^{-1}, $L_{\nu_\mu} = 0.5 \times L_{\nu_e,\bar\nu_e}$, $T_{\nu_e} = 4$ MeV, $T_{\bar\nu_e} = 5$ MeV, and $T_{\nu_\mu} = 10$ MeV.

In Table 1, we compare the heating rates per baryon for light nuclei, which can be evaluated without referring to the matter profiles. We set $r = 100$ km, $L_{52} = 5.0$, and $X_i = 1.0$. Note that the cooling rates are not subtracted here for comparison. We set $X_p = X_n = 0.5$ in the evaluation of the heating rates for nucleons. We find that deuterons have heating rates per baryon that are comparable to those of nucleons. Tritons, helions, and alpha particles have rather small heating rates per baryon. Muon neutrinos do not heat nucleons but rather light nuclei through the NC, since the former have no internal degree of freedom that can be excited.

3.1. Steady State

The left panel of Figure 1 shows shock radius r_s versus the mass accretion rate $\dot M_{\rm sun}$ in the case of spherically symmetric, steady accretion flows with and without heating of light nuclei for $L_{52} = 5.2$ and 6.2. We can see the that shock radii are not significantly affected by this change. Higher luminosities and lower mass accretion rates increase the influence of the light nuclei on the structures of the steady states. Note also that higher luminosities and lower mass accretion rates result in steady states that are closer to the critical states; small variations may have a greater effect. The center and right panels of Figure 1

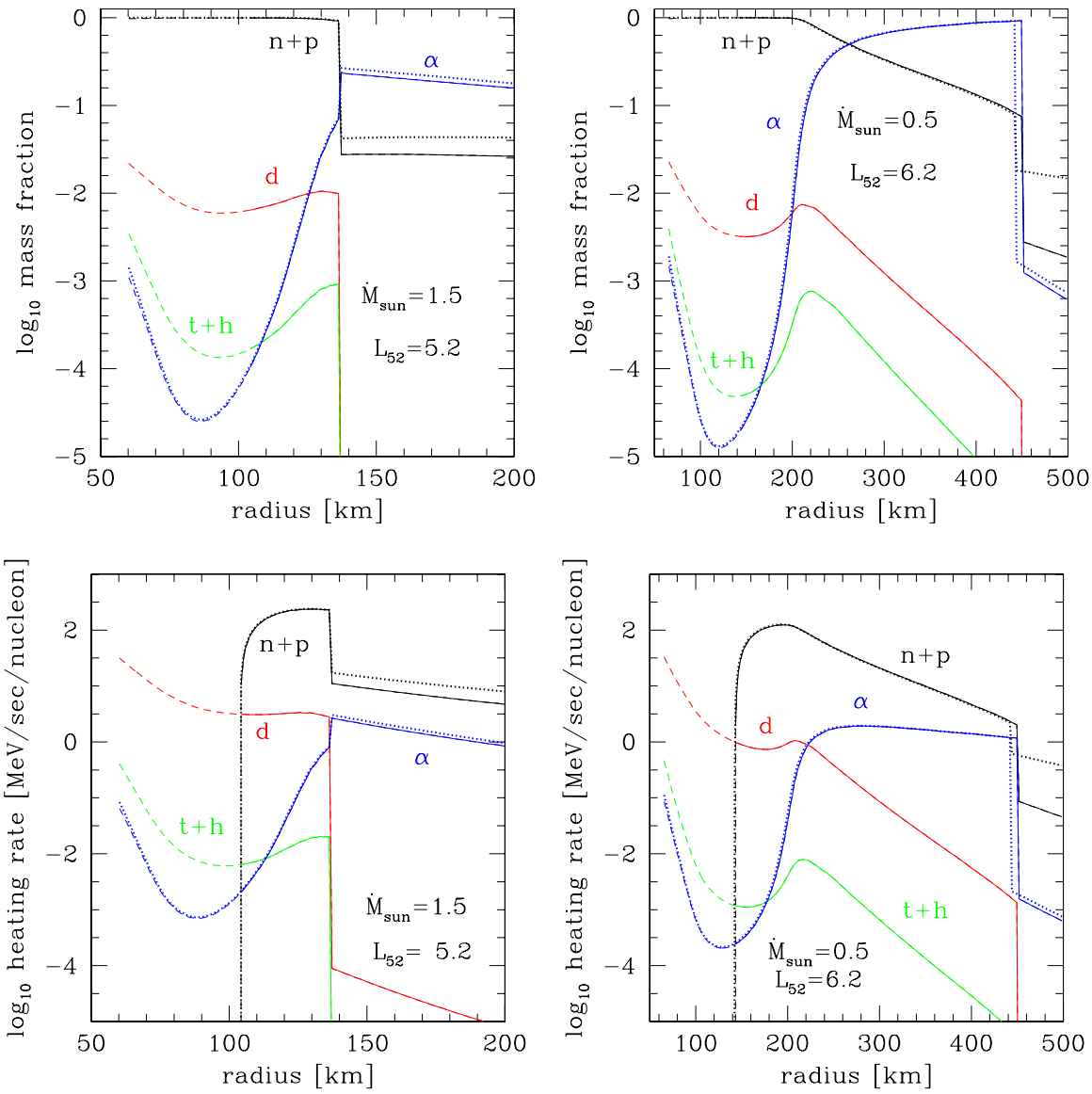

Figure 2. Mass fractions (upper panels) and heating rates per baryon (bottom panels) for $A_i = 1$: protons and neutrons (black), $A_i = 2$: deuterons (red), $A_i = 3$: tritons and helions (green), and $A_i = 4$: alpha particles (blue) for $L_{52} = 5.2$ with $\dot{M}_{\rm sun} = 1.5$ (left panel) and $L_{52} = 6.2$ with $\dot{M}_{\rm sun} = 0.5$ (right panel). Dashed lines indicate the cooling regions where the cooling reaction of nucleons is dominant. Dotted lines are the results of the models with Shen's EOS for the same L_{52} and $\dot{M}_{\rm sun}$. (A color version of this figure is available in the online journal.)

show the variations of the shock radii, which are defined as $(r_s - r_{s0})/r_{s0} \times 100$ [%], with the shock radius r_{s0} corresponding to no light-nuclei heating. We plot three cases, in which we include either the heating of all light nuclei or that of only the deuterons or alpha particles, respectively. The results indicate that deuterons are always one of the main contributors to the heating, although the resultant variations are not so large. On the other hand, alpha particles can push the shock wave only when the mass accretion rate is small. The nuclei with $A_i = 3$ have little influence under any condition, since tritons and helions are much less abundant than the other two light nuclei.

Figure 2 shows the profiles of the mass fraction and the heating rate of each nuclear species for two models, which include heating by all the light nuclei. For the model with $L_{52} = 5.2$ and $\dot{M}_{\rm sun} = 1.5$, the shock radius is ~140 km and the heating by deuterons is second most dominant after that of the nucleons in the gain region. The gain region refers to the region between the gain radius r_g and shock radius r_s. The gain radius r_g is defined as the radius at which the neutrino heating is equal to the neutrino cooling and there is no net energy gain. For the model with $L_{52} = 6.2$ and $\dot{M}_{\rm sun} = 0.5$, alpha particles, as well as nucleons in the outer part of the gain region, contribute to the heating. This difference between deuterons and alpha particles can be also seen in Figure 3, which shows T–ρ plane assuming that $Y_e = 0.5$. Regions where deuterons and alpha particles are abundant on the plot are indicated. Superimposed are the actual (T, ρ) values obtained in the gain region. Note that the electron fractions obtained in the simulations have various values between 0.3 and 0.5 in the gain region. However, the deuteron-rich and alpha-rich regions for $Y_e = 0.3$ are not much different from those for $Y_e = 0.5$.

For the model with $L_{52} = 6.2$ and $\dot{M}_{\rm sun} = 0.5$ (brown line), the shock radius is rather large and the plots of (T, ρ) pairs obtained in this model extend to lower densities and temperatures, which favor the existence of alpha particles. For

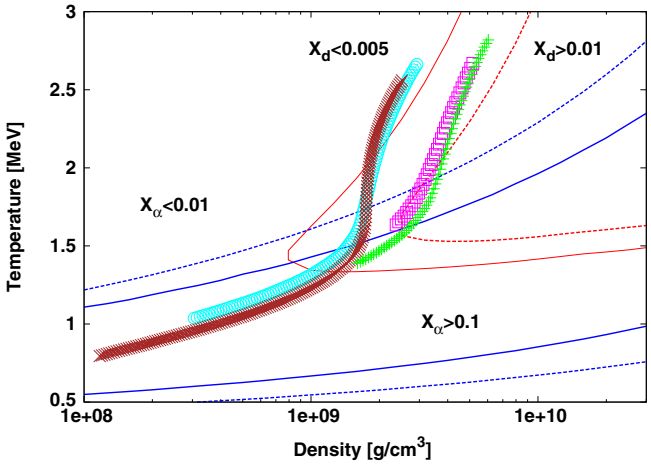

Figure 3. Temperature vs. density. The lines show the contours of the mass fractions of deuterons X_d and alpha particles X_α at $Y_e = 0.5$ (red thin lines for $X_d = 0.005$, red dashed lines for $X_d = 0.01$, blue dashed lines for $X_\alpha = 0.01$, and blue solid lines for $X_\alpha = 0.1$). The symbols correspond to the densities and temperatures in the gain regions for $L_{52} = 5.2$ and $\dot{M}_{\rm sun} = 0.5$ (cyan) and $\dot{M}_{\rm sun} = 1.5$ (magenta) and $L_{52} = 6.2$ and $\dot{M}_{\rm sun} = 0.5$ (brown) and $\dot{M}_{\rm sun} = 1.5$ (green).

(A color version of this figure is available in the online journal.)

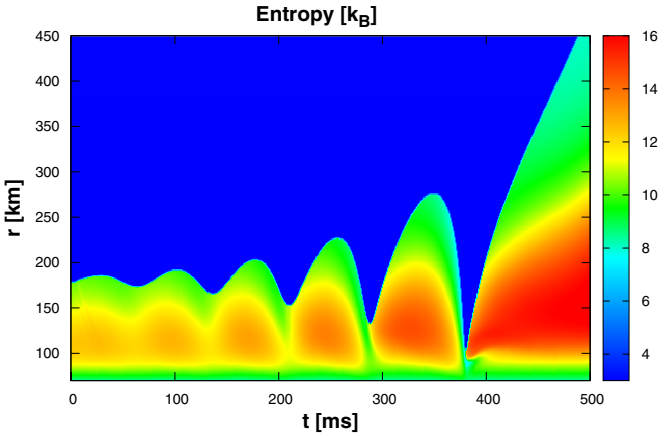

Figure 4. Entropy per baryon in the (r, t) plane for the 1D model with $L_{52} = 5.4$ and $\dot{M}_{\rm sun} = 1.0$.

(A color version of this figure is available in the online journal.)

the model with $L_{52} = 5.2$ and $\dot{M}_{\rm sun} = 1.5$ (magenta line), on the other hand, all the (T, ρ) pairs are outside the region in which the fraction of alpha particles is larger than 10% and are located close to the region in which a deuteron fraction of more than 1% is realized. Note that deuterons have energy-transfer coefficients more than 10 times larger than those of alpha particles, as shown in Table 1. Deuterons can hence make some small contributions to the total heating rates even if their fraction is as small as ∼1%. Deuterons and alpha particles can contribute to the neutrino heating in the inner and outer parts of the gain region, respectively. As a result, the larger shock radius leads to more efficient heating by alpha particles than by deuterons.

So far, we have investigated the differences that heating via light nuclei may make by arbitrarily switching them on and off for the same background models. It is interesting, however, to make comparisons against the models in which not only the heating but also the existence of light nuclei other than alpha particles is entirely neglected. There are two reasons for this proposition: first, the EOSs that have been commonly employed in supernova simulations thus far consider only alpha particles as light nuclei; second, if light nuclei did not exist in the first place, nucleons would be more populous, taking their place; the nucleons could be efficiently heated and thus reduce or even nullify the differences we have observed above.

In order to see this scenario we employ Shen's EOS (Shen et al. 2011b), one of the standard EOSs for supernova simulations in which only alpha particles are included as light nuclei. We construct spherically symmetric, steady accretion flows and investigate the differences that d, t, and h make. Strictly speaking, there are some differences between our EOS and Shen's EOS other than their treatment of light nuclei. For example, Shen's EOS takes into account a single representative heavy nucleus whereas our EOS handles an ensemble of nuclei. This difference is not so important in the post-shock region that we are concerned with, however, since the nucleons and light nuclei are dominant there. Even the treatment of alpha particles is different between the two EOSs, since we take into account the effects of ambient matter when evaluating the mass of alpha particles (Furusawa et al. 2013). This difference, however, manifests itself only at high densities, $\rho \gg 10^{11}$ g cm^{-3}, the density at the inner boundary of our models.

Figure 2 shows that the abundances of nucleons and alpha particles are almost identical between the corresponding models. As a result, the heating via nucleons does not differ significantly, although both the mass fractions and the heating rates of nucleons and alpha particles are slightly larger in the model with Shen's EOS. For instance, the mass fractions of nucleons and alpha particles in the model with our EOS are smaller by 0.9% and 0.3%, respectively, than those in the model with Shen's EOS at $r = 130$ km for $L_{52} = 5.2$ and $\dot{M}_{\rm sun} = 1.5$. This difference is due to the existence of light nuclei other than alpha particles. The heating rates per baryon (Q_E, Q_α) are (237.0, 0.3643) MeV s^{-1} with our EOS, compared with the values (238.6, 0.3653) MeV s^{-1} that are obtained with Shen's EOS. The total heating rate, $Q_E + Q_d + Q_t + Q_h + Q_\alpha$, in the model with our EOS, however, is larger than the sum of Q_E and Q_α in the model with Shen's EOS because of the contribution from deuterons, $Q_d = 3.264$. As a result, the shock radius in our model is slightly larger than that in Shen's model. The difference is clearer in the case of $L_{52} = 6.2$ and $\dot{M}_{\rm sun} = 0.5$. To be fair, we point out that Q_E includes cooling but Q_d, Q_t, Q_h, and Q_α do not completely (see Section 2). If we compare the absorption of neutrinos alone, the total rates are larger in the models with Shen's EOS, since the contribution from nucleons overwhelms that from deuterons. Comparisons in dynamical contexts will be given later.

3.2. 1D Simulations

To obtain the basic features of heating by light nuclei in dynamical settings, we perform a spherically symmetric 1D simulation. We employ 300 radial mesh points as explained in Section 2. Figure 4 shows the entropy evolution of the model with $L_{52} = 5.4$ and $\dot{M}_{\rm sun} = 1.0$. Although we do not add any perturbations initially, numerical noise induces small radial oscillations that grow gradually. It can be seen that the matter just below the shock wave has a low entropy when the shock radius is large. It should be also noted that the entropy of the same shock radius is smaller when the shock is receding than when it is advancing. This asymmetric feature becomes clearer as the shock radius gets larger. In Figure 5, we compare the time evolution of the integrated heating rate of each nuclear

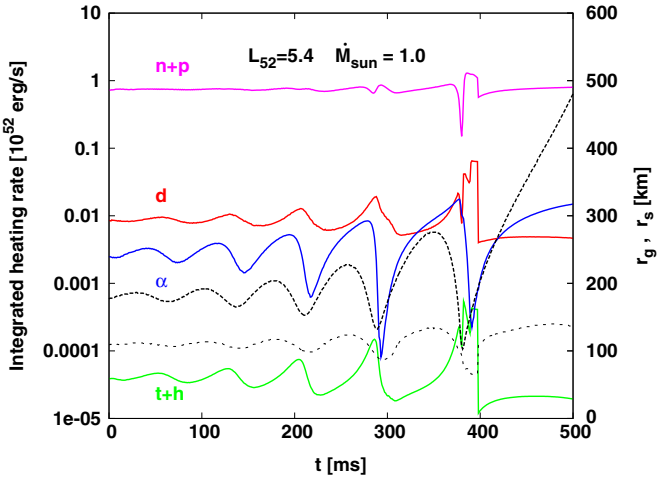

Figure 5. Time evolution of the average shock and gain radii and integrated heating rates of different nuclear species. Black dashed and dotted lines denote the shock and gain radii, respectively. Magenta, red, green, and blue lines represent the heating rates of $A_i = 1$ (nucleons), $A_i = 2$ (deuterons), $A_i = 3$ (tritons and helions), and $A_i = 4$ (alpha particles), respectively.

(A color version of this figure is available in the online journal.)

species along with the shock and gain radii. The shock radius is defined as the iso-entropic surface of $s = 5.0\,k_B$, where k_B is the Boltzmann constant. The heating rates are integrated over the gain region as $\int_{\rm gain} Q_i d\mathbf{r}^3$ and given in units of 10^{52} erg s^{-1}. We can see that the heating rate of alpha particles changes roughly in step with the shock radius, since a larger shock radius leads to a larger fraction of alpha particles. The peak time in the heating rate of alpha particles is delayed from the time of the local maximum in the shock radius because of the asymmetric feature in the entropy mentioned above. We also find that the heating of alpha particles is more important than that of deuterons after the shock wave revives and proceeds outward ($t > 400$ ms). On the other hand, the heating rates of deuterons reach a local maximum when the gain and shock radii are small, since matter has a high density and favors deuterons. Furthermore, since deuterons are located closer to the neutrino sphere, they attain heating rates as high as 1%–10% of those of nucleons. These results indicate that alpha particles and deuterons heat matter in different phases in the oscillation of the shock wave. Although tritons and helions are similar to deuterons, they are quite minor contributors.

3.3. 2D Simulations

Figure 6 displays the time evolution of the average shock radii for four models in which all light nuclei, only deuterons,

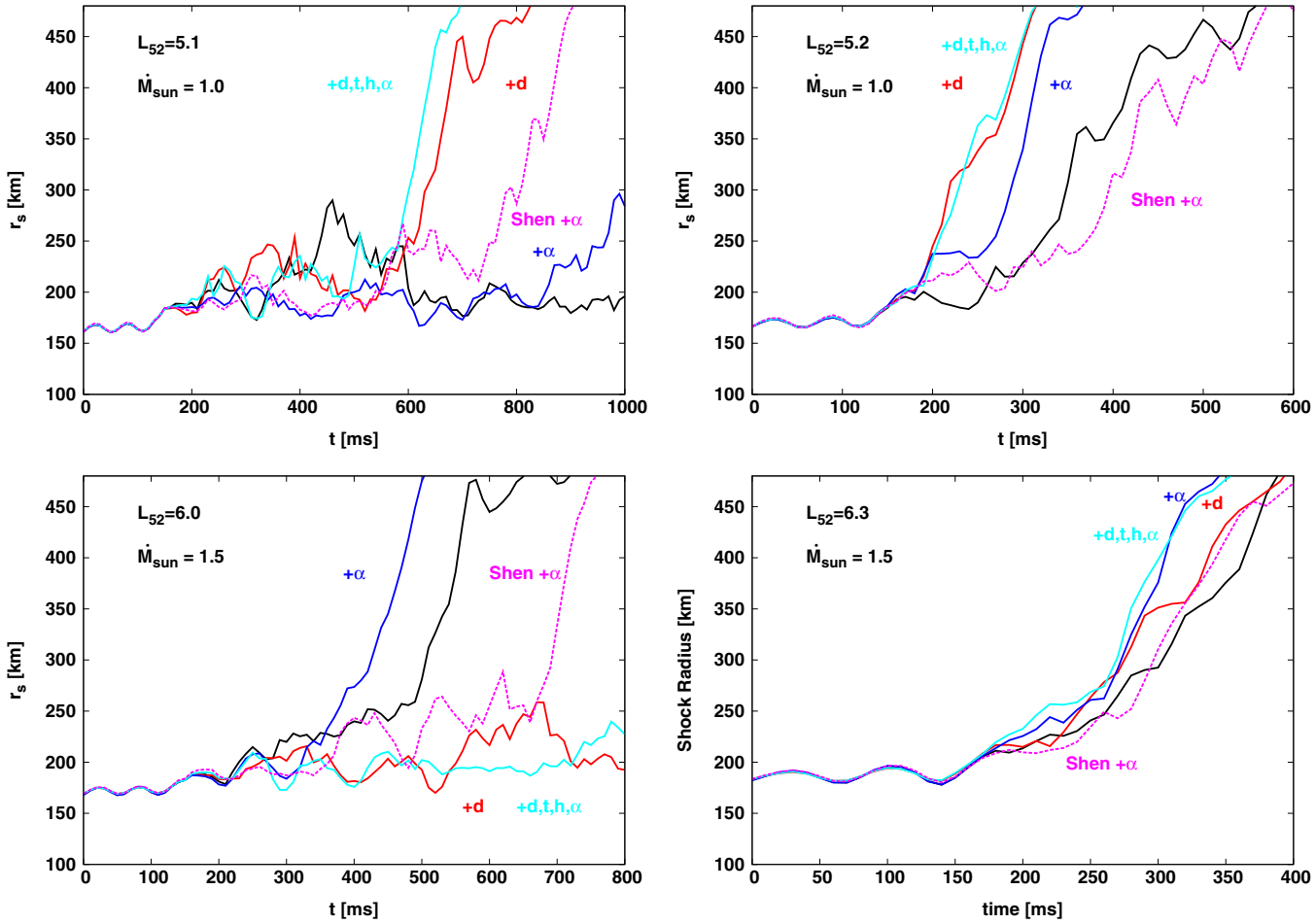

Figure 6. Time evolution of the average shock radii for the models with the heating of all light nuclei (cyan solid lines), only deuterons (red solid lines), only alpha particles (blue solid lines), and no light nuclei (black solid lines), as well as the models with Shen's EOS and the heating of alpha particles (magenta dashed lines). The combinations of the luminosity and mass accretion rate are $L_{52} = 5.1$ and 5.2 with $\dot{M}_{\rm sun} = 1.0$ and $L_{52} = 6.0$ and 6.3 with $\dot{M}_{\rm sun} = 1.5$.

(A color version of this figure is available in the online journal.)

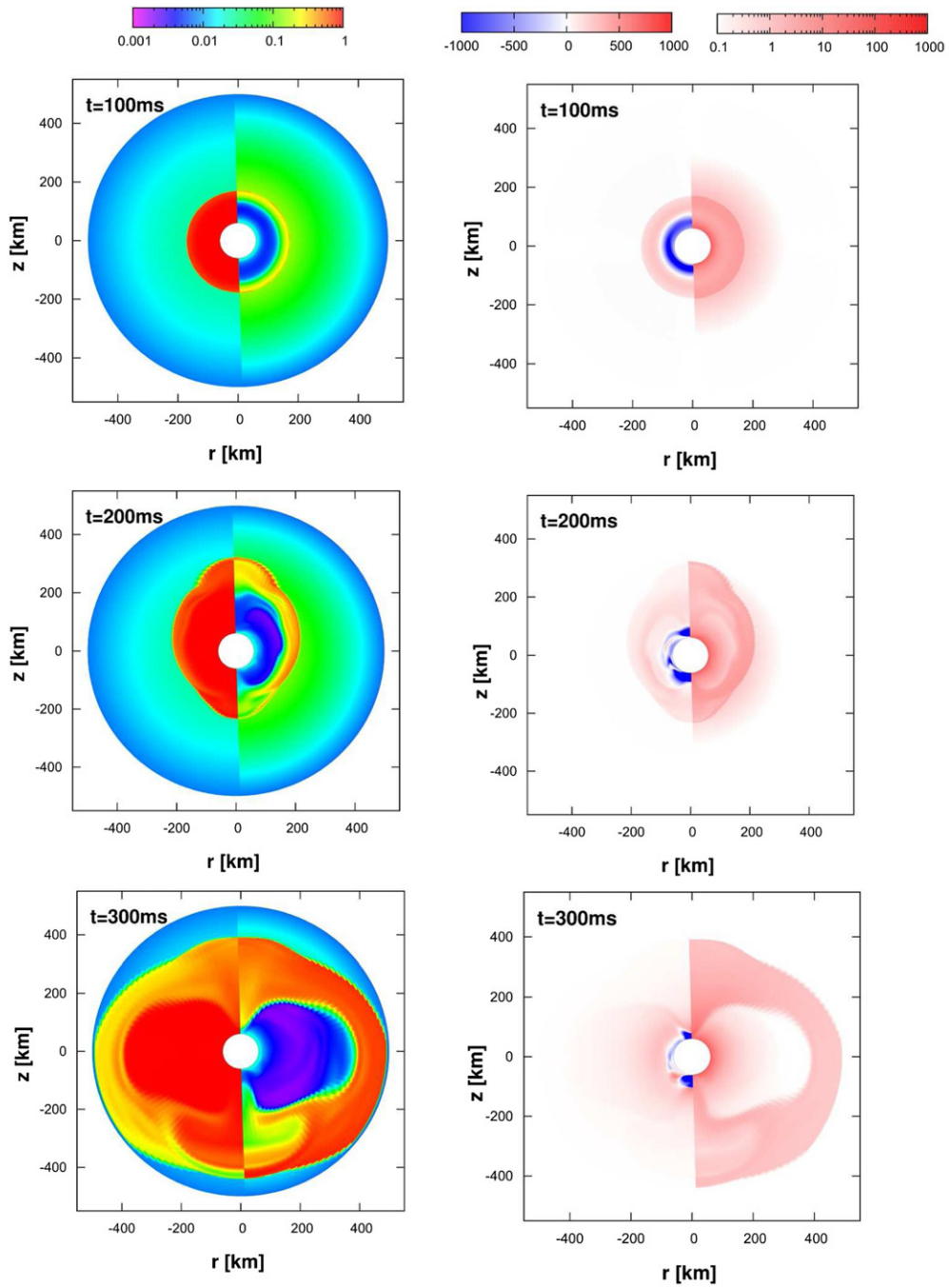

Figure 7. Mass fractions of nucleons, $X_n + X_p$ (left halves of left panels), those of all light nuclei, $X_d + X_t + X_h + X_\alpha$ (right halves of left panels), the heating and cooling rates per baryon in units of MeV s^{-1} of nucleons, $Q_E \times m_u/\rho$ (left halves of right panels), and those of all light nuclei, $(Q_d + Q_t + Q_h + Q_\alpha) \times m_u/\rho$ (right halves of right panels). The times are $t = 100$, 200 and 300 ms and the luminosity and accretion rate are $L_{52} = 5.2$ and $\dot{M}_{\rm sun} = 1.0$.

(A color version of this figure is available in the online journal.)

only alpha particles, and no light nuclei, respectively, are taken into account as heating sources. The results of the model, in which we employ Shen's EOS and take into account heating via alpha particles, are also shown and discussed later. The models without deuteron heating do not succeed in the shock revival for $L_{52} = 5.1$, whereas the other two models do, although more time is required. For $L_{52} = 5.2$, on the other hand, all models produce shock revival. We can see that heating by deuterons and alpha particles both reduce the time to shock revival. The same trend is also seen in the models with $L_{52} = 6.3$ and $\dot{M}_{\rm sun} = 1.5$. These results suggest that the heating of light nuclei, especially deuterons, is helpful for shock revival. Note, however, that this conclusion may be too naive, since the time to shock revival is known to be sensitive to various ingredients such as the initial perturbations when the neutrino luminosity is close to the critical value. In fact, the models with $L_{52} = 6.0$ and $\dot{M}_{\rm sun} = 1.5$ show the opposite trend when we include deuteron- heating: the models without the deuteron heating gain more energy through nucleon heating alone than do other models. This result is because the deuteron heating prevents the shock wave from shrinking in the first place and reduces the heating via nucleons, since matter tends to be farther

away from the neutrino sphere. For instance, at $t = 210$ ms, when all the models with $L_{52} = 6.0$ and $\dot{M}_{\rm sun} = 1.5$ reach a local minimum in their average shock radius, the values of the average shock radius and the angle-averaged heating rate per baryon for nucleons are 178 km and 223 MeV s^{-1}, respectively, in the model without light nuclei heating. On the other hand, these values are 183 km and 211 MeV s^{-1} in the model with only deuteron heating. Although we cannot find a clear trend when deuteron heating is helpful for shock revival, heating by deuterons is non-negligible regardless. Alpha particles do not work that way, on the other hand. They heat matter when the shock wave has a large radius, as discussed in Section 3.2. As a result, alpha particles do not affect the shock recession. The model with the alpha-particle-heating alone has almost the same shock radius, 177 km, at $t = 210$ ms. Heating via alpha particles is hence always favorable for shock revival whenever it is effective.

Comparisons between models with our EOS and Shen's EOS are a bit more difficult due to the inherent intricacies of shock revival mentioned above. We can recognize some trends in Figure 6, however. As noted in Section 3.1, heating via nucleons alone is larger in models with Shen's EOS whereas the total heating rates are greater for the models with our EOS thanks to the contribution from deuterons. In accordance with this result, shock revival occurs earlier in the models that employ our EOS and incorporate heating via deuterons than in the corresponding models with Shen's EOS. The order is reversed in some cases if the heating of deuterons is switched off in the models with our EOS. For example, the stalled shock is revived at $t \sim 800$ ms for Shen's EOS in the case of $L_{52} = 5.1$; for our EOS, revival happens at $t \sim 600$ ms if the heating of deuterons is included, whereas the shock remains stalled even at $t \sim 1000$ ms if the heating of deuterons is turned off. In the same way, the model with Shen's EOS for $L_{52} = 6.0$ shows an intermediate time evolution between the models that employ our EOS with and without deuteron heating. It should be remembered, however, that other differences such as the preheating of nucleons ahead of the shock wave may have some influence on the results.

We now focus on the model with $L_{52} = 5.2$ and $\dot{M}_{\rm sun} = 1.0$ that includes heating by all light nuclei to explore in more detail the role of light nuclei in the evolution of the shock wave. The shock oscillation grows linearly by $t \sim 150$ ms in this model, as seen in Figure 6. The distributions of nucleons and light nuclei are almost spherically symmetric at $t = 100$ ms, as seen in the upper panels of Figure 7. The heating rates of light nuclei are large in the narrow region near the quasi-steady shock wave at $t = 100$ ms. At $t = 200$ and 300 ms, however, we observe the deformed shock waves that have reached the non-linear regime of the SASI. In some regions, the light nuclei are indeed abundant and their heating is accordingly efficient. Figure 8 shows the pairs of (T, ρ) obtained along five different radial rays (see Figure 3). Although these pairs—the black symbols—are not initially located in regions that are rich in light nuclei, turbulence in the non-linear SASI broadens the distributions. Figure 9 shows the mass fractions and the heating rates of different nuclear species along two radial rays with [$\theta = 180^\circ$ at $t = 200$ ms] and [$\theta = 0^\circ$ at $t = 300$ ms]. The heating rate of deuterons becomes as high as $\sim$10% of that of nucleons at $t = 200$ ms around the bottom of the gain region. It should be noted that the cooling is subtracted for nucleons in Q_E, whereas it is not included in $Q_{d,t,h,\alpha}$ because of the lack of rates in the literature. There are indeed large cancellations between heating and cooling at the bottom of the

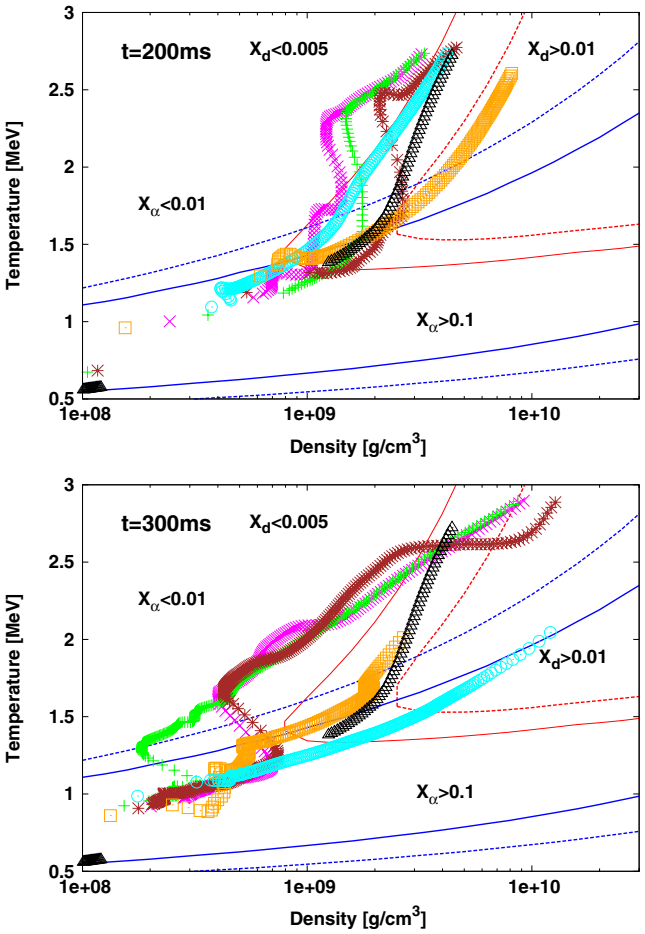

Figure 8. Lines are the same as in Figure 3. The symbols show the densities and temperatures in the gain regions at $t = 200$ ms (upper panel) and 300 ms (lower panel) for the radial rays with $\theta = 0^\circ$ (cyan), 45° (magenta), 90° (green), 135° (brown), and 180° (orange). The black symbols correspond to the initial spherically symmetric state.

(A color version of this figure is available in the online journal.)

gain regions. For instance, the heating and cooling rates per baryon for nucleons are 631 and -584 MeV s^{-1} per baryon at $r = 110$ km along the radial ray with $\theta = 180^\circ$ at $t = 200$ ms. If we compare the pure heating rates, deuterons have 4.73 MeV s^{-1} per baryon, which is just 0.75% of the pure heating rate for nucleons in the same example. Around the same time, the shock wave moves northward ($\theta = 0^\circ$) and the matter in the southern part ($\theta = 180^\circ$) goes down deep into the central region. The orange symbols in the top panel of Figure 8 indicate that the matter in this southern part has low entropies, resulting in more deuterons near the bottom of the gain region than the matter in other parts. At $t = 300$ ms, the shock wave reaches $\sim$400 km and the heating of alpha particles is dominant for the same reasons we explained in Figure 2. We can see in the bottom panel of Figure 8 that the matter along the radial ray with $\theta = 0^\circ$ has also lower entropies; as a consequence, deuterons and alpha particles are abundant in the regions of high and low densities, respectively. At both $t = 200$ and $t = 300$ ms, deuterons have heating rates comparable to those of nucleons near the bottom of the gain regions. The heating rates of alpha particles are $\sim$10% of those of nucleons around the shock wave.

Figure 10 displays the time evolution of the integrated heating rate of each nuclear species together with the shock and gain radii along two radial rays with $\theta = 0^\circ$ and 90°.

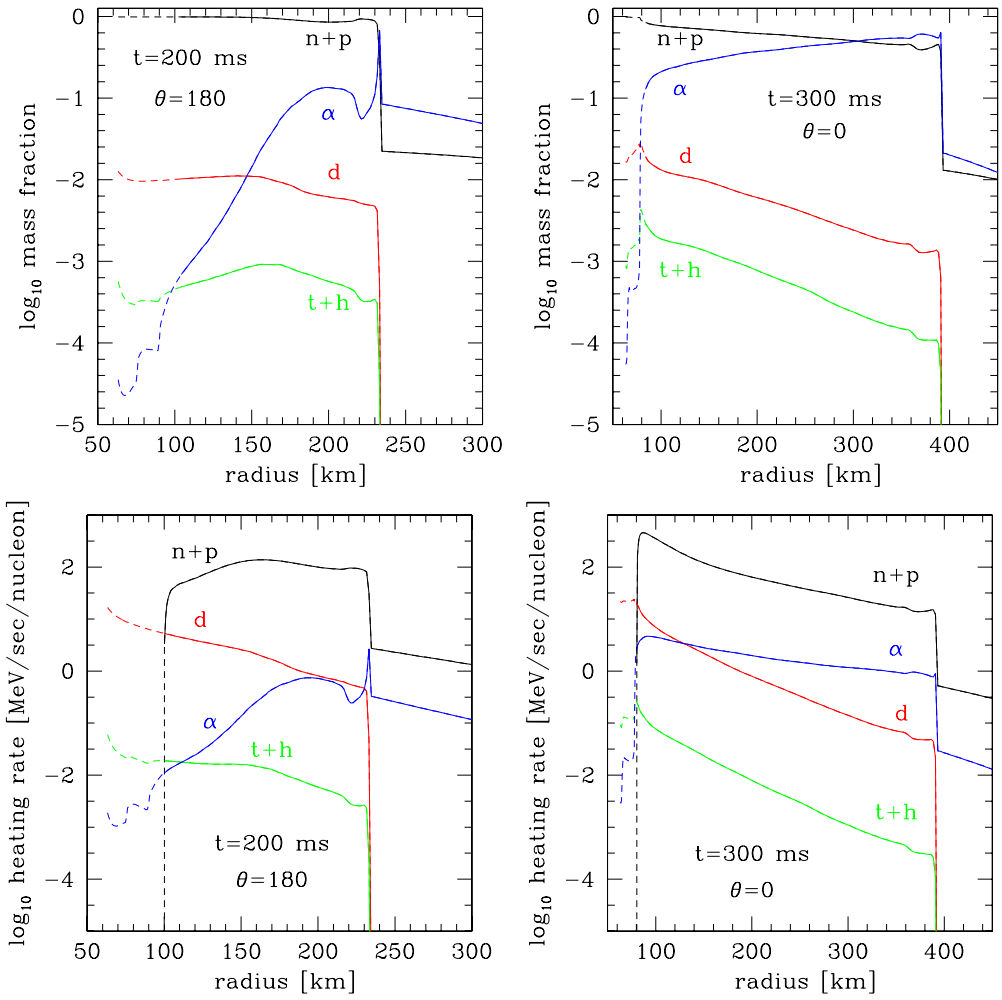

Figure 9. Mass fractions (upper panels) and heating rates per baryon (lower panels) along the radial rays with $\theta = 180°$ at $t = 200$ ms (left panels) and with $\theta = 0°$ at $t = 300$ ms (right panels). The notations of various lines are the same as in Figure 2.

(A color version of this figure is available in the online journal.)

The integrated heating rate for a specific direction is calculated as $4\pi \int_{r_g(\theta)}^{r_s(\theta)} Q_i(r,\theta) r^2 dr$ in the same way as for the 1D model in Figure 5. The heating rates of deuterons and alpha particles are about 1% and 0.1%, respectively, of those of nucleons in the linear phase of the SASI. However, both of these rates are much more efficient in the subsequent non-linear evolution of the SASI and shock revival. We can see that deuterons and alpha particles have different temporal variations in heating rates, which are ascribed to the fact that they occupy different parts of the gain region, as explained in Section 3.2. Note that the heating of light nuclei occurs quite inhomogeneously and that the local heating can be more efficient than the average, as shown in Figure 9.

In the models explored so far, the temperature of ν_μ is assumed to be 10 MeV. However, this value may be too high. In fact, recent simulations tend to predict temperature of ν_μ to be much closer to those of ν_e and $\bar{\nu}_e$ (e.g., Janka 2012). We hence repeat some simulations with $T_{\nu_\mu} = 5$ MeV. As shown in Table 1, the ν_μ-heating rate per baryon is reduced by a factor of 10. The decrease in the net heating rates is particularly severe for tritons, helions, and alpha particles, since the NC interactions with ν_μ are dominant for the heating of these species. On the other hand, the total heating rates of deuterons are reduced by only 24% because the CC interactions with ν_e and $\bar{\nu}_e$ are more important.

Figure 11 shows the temporal evolution of the average shock radii for the models with $L_{52} = 5.2$ and $\dot{M}_{\rm sun} = 1.0$, the counterparts of those models presented in Figure 6. The results are qualitatively different. In fact, shock revival occurs earlier without the heating of deuterons, although the shock radius is larger at $t \sim 200$ ms with the deuteron heating. This result occurs because heating of nucleons is reduced in the presence of deuterons during the shock expansion at $t \sim 200$ ms, which is similar to what we observed in the models for $T_{\nu_\mu} = 10$ MeV with $L_{52} = 6.0$ presented in Figure 6. The difference between the models with and without alpha particles is smaller for $T_{\nu_\mu} = 5$ MeV than for $T_{\nu_\mu} = 10$ MeV. Figure 12, the counterpart of Figure 9, displays the mass fractions and heating rates of different light nuclei along the radial ray with $\theta = 180°$ at $t = 200$ ms. Although the dynamics are stochastic owing to the turbulence induced by the SASI and the shock positions are different between the models with $T_{\nu_\mu} = 5$ MeV and $T_{\nu_\mu} = 10$ MeV, the heating by deuterons is not significantly decreased thanks to the CC contributions, whereas the heating rates of alpha particles are decreased by a factor of 10. Provided the high energy-dependence of the ν_μ-heating, we think that our standard models with $T_{\nu_\mu} = 10$ MeV give the upper limit on the ν_μ-heating whereas the models with $T_{\nu_\mu} = 5$ MeV set the lower limit.

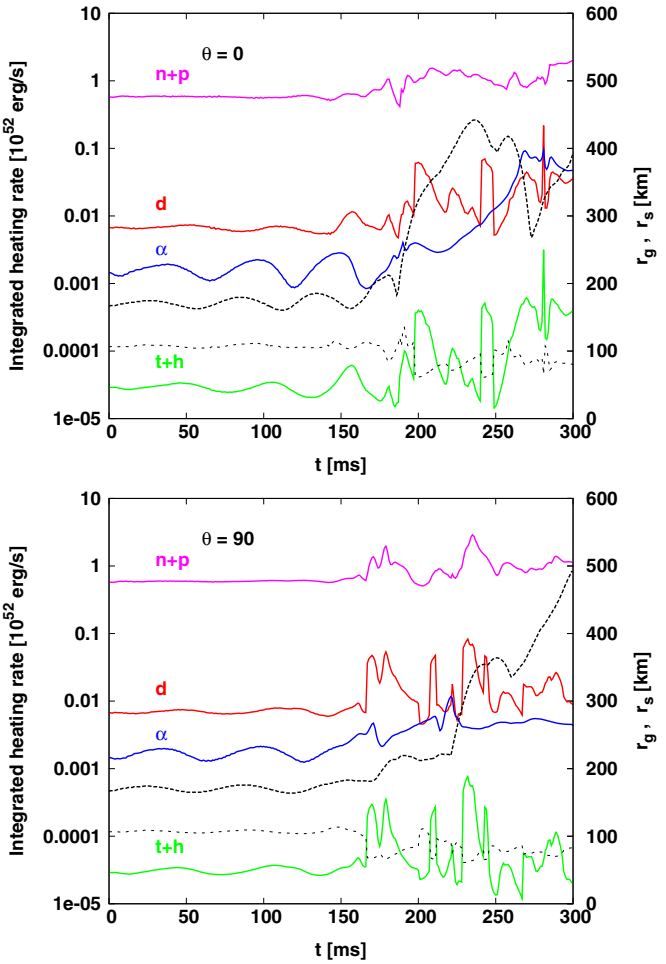

Figure 10. Time evolution of the shock and gain radii and integrated heating rates on the radial rays with $\theta = 0^\circ$ (upper panel) and $\theta = 90^\circ$ (lower panel). The notations of various lines are the same as in Figure 5.

(A color version of this figure is available in the online journal.)

In our standard models, the CC interactions with light nuclei are ignored in the temporal evolution of the electron fraction. One may be worried, however, that this assumption could affect the dynamics, since the CC interactions are dominant in the heating of deuterons. Note that the CC contributions are much smaller for t, h, and α. In order to address this issue, we have included the contributions of deuterons and tritons in Equation (4); the contribution of deuterons is given by:

$$Q_{Nd} = X_d \frac{31.6\,\mathrm{s}^{-1}}{(r/10^7\,\mathrm{cm})^2}\left[\frac{L_{\nu_e}}{10^{52}\,\mathrm{erg\,s}^{-1}}\left(\frac{5\,\mathrm{MeV}}{T_{\nu_e}}\right)\frac{A_d^{-1}\langle\sigma^+_{\nu_e}\rangle_{T_{\nu_e}}}{10^{-40}\,\mathrm{cm}^2}\right.$$
$$\left. - \frac{L_{\bar{\nu}_e}}{10^{52}\,\mathrm{erg\,s}^{-1}}\left(\frac{5\,\mathrm{MeV}}{T_{\bar{\nu}_e}}\right)\frac{A_d^{-1}\langle\sigma^-_{\bar{\nu}_e}\rangle_{T_{\bar{\nu}_e}}}{10^{-40}\,\mathrm{cm}^2}\right]. \quad (7)$$

This expression was obtained by simply replacing the energy-transfer coefficient $\langle\sigma_\nu^\pm E_\nu\rangle_{T_\nu}$ with the cross section averaged over the neutrino spectrum, $\langle\sigma_\nu^\pm\rangle_{T_\nu}$, in Equation (5). We ignore the other contributions. For tritons, only the electron-type anti-neutrinos are included, since the cross section for ν_e is currently unavailable. Note, however, that the contribution of tritons is negligible anyway, as will be shown shortly.

We initially constructed spherically symmetric, steady accretion flows and then performed 2D simulations incorporating Q_{Nd} and Q_{Nt}. The neutrino luminosity and mass accretion rate were fixed to $L_{52} = 5.2$ and $\dot{M}_{\rm sun} = 1.0$ here. It turns out that the temporal evolution of the shock wave is unchanged from that presented in Figure 6, which justifies neglecting of these effects in the standard models. In fact, Figure 13 compares Q_{Nd} and Q_{Nt} with Q_N, the contribution of nucleons, at $t = 0$ and 200 ms and demonstrates that Q_{Nd} is about 0.1% of Q_N in most regions and Q_{Nt} is always negligibly small. Although we can see at initial times a slight increase in Y_e when Q_{Nd} and Q_{Nt} are included, the difference disappears by $t = 200$ ms.

The reasons why deuterons are non-negligible heating sources (providing 1%–10% of the nucleon contributions) yet not significant contributions to the evolution of Y_e can be listed as the following: (1) the net heating rate of nucleons, Q_E, is an outcome of rather large cancellations between heating and cooling near the gain radius whereas such cancellations are not so large in Q_N; as a result Q_N is much greater than Q_{Nd} in the region where the deuteron-heating is efficient; (2) the evolution of Y_e is controlled by the competition between the electron-type neutrinos and anti-neutrinos; according to the current formula, Q_{Nd} is given as $Q_{Nd} = Q_{Nd}(\nu_e d) - Q_{Nd}(\bar{\nu}_e d) = 0.188\ Q_{Nd}(\nu_e d)$ and the cancellation is much larger than for Q_N; (3) the NC reactions contribute 12% and 33% to Q_d for $T_{\nu_\mu} = 5$ and $T_{\nu_\mu} = 10$ MeV, respectively, but none to Q_{Nd}.

To summarize, the heating via light nuclei is non-negligible in the non-linear phase of the SASI, in which various values of (T, ρ) are realized. On the other hand, heating via light nuclei is minor in the linear stage. Among light nuclei, deuterons play important roles near the bottom of the gain region whereas alpha particles are influential near the shock fronts when the shock wave is expanding and, as a consequence, the densities and temperatures become lower. The results are rather sensitive to the ν_μ spectrum. If the temperature of ν_μ is as low as that of $\bar{\nu}_e$, the heating of alpha particles will be substantially diminished whereas the deuteron heating will not by reduced as much.

4. SUMMARY AND DISCUSSIONS

We have investigated the influence of the inelastic interactions of neutrinos with light nuclei on the dynamics in the post-bounce phase of core-collapse supernovae. We have run 2D numerical simulations of the SASI under the assumption of axial symmetry for some representative combinations of luminosity and mass accretion rate. We have not solved the dynamics of the central part of the core and have instead replaced it with suitable boundary conditions. We have started the simulations from a spherically symmetric steady state, adding some perturbations to the radial velocity. The neutrino transport was handled by the simple light-bulb approximation with a time-independent Fermi–Dirac spectrum. In addition to the ordinary heating and cooling reactions with nucleons, we have also taken into account, for the first time, the heating reactions with four light nuclei. The abundance of light nuclei is provided by the multi-nuclei EOS together with other thermodynamical quantities.

We have found that the evolution of shock waves in 2D is influenced by the heating of deuterons and alpha particles and that these species have different roles. In the initial steady state, the heating by light nuclei is the most efficient for the combination of high neutrino luminosity and low mass accretion rate, since the shock radius is large and the matter near the shock front has the low densities and temperatures that yield a large amount of alpha particles. On the other hand, deuterons are populous near the bottom of the gain region, where matter has higher densities and temperatures. Deuterons hence have some

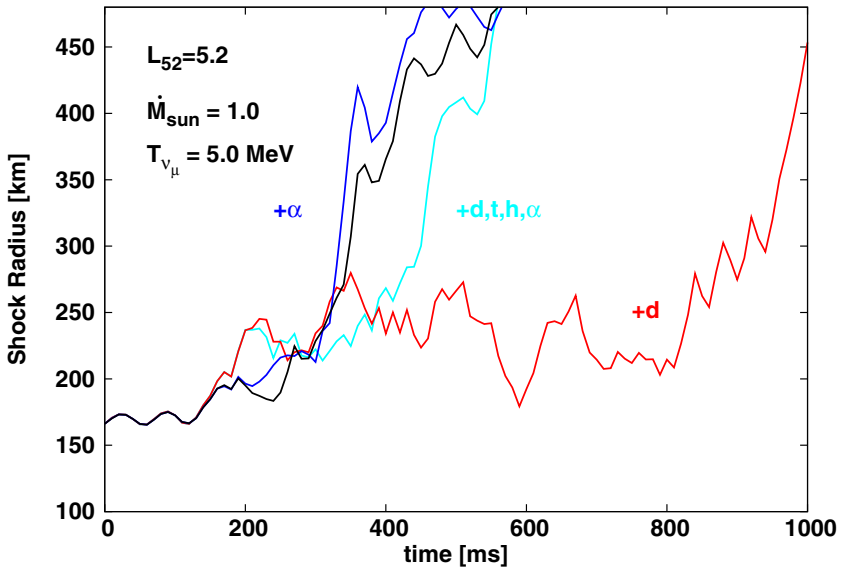

Figure 11. Time evolution of the average shock radii for the models with the heating of all light nucleus (cyan line), only deuterons (red line), only alpha particles (blue line), and no light nuclei (black line). The temperature of ν_μ is $T_{\nu_\mu} = 5$ MeV and the luminosity and mass accretion rate are $L_{52} = 5.2$ and $\dot{M}_{\rm sun} = 1.0$, respectively.
(A color version of this figure is available in the online journal.)

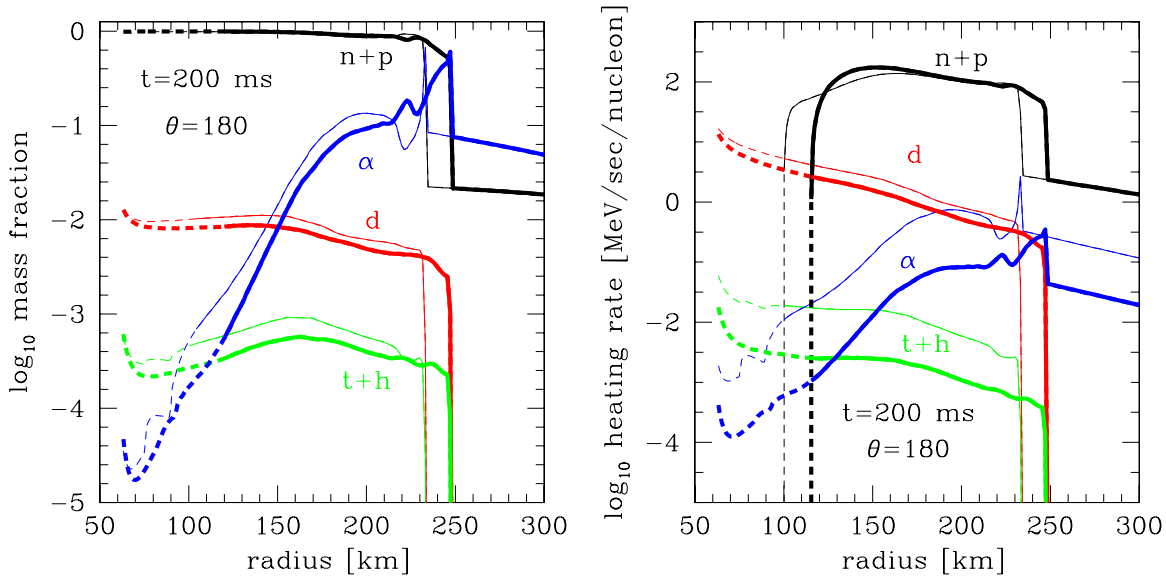

Figure 12. Mass fractions (left panel) and heating rates per baryon (right panel) along the radial ray with $\theta = 180^\circ$ at $t = 200$ ms for $T_{\nu_\mu} = 5$ MeV (thick lines) and $T_{\nu_\mu} = 10$ MeV (thin lines). The thin lines are the same as those in the left panels of Figure 9 and the notations of the lines are also identical to those in Figure 9.
(A color version of this figure is available in the online journal.)

impact on the shock radius regardless of neutrino luminosity and mass accretion rate. From the results of 1D simulations, we found that the integrated heating rates of deuterons and alpha particles become high at different phases in the oscillations of shock wave: the heating rate of deuterons becomes the highest when the shock radius reaches a minimum and the matter compression is the greatest. While heating via deuterons is constantly effective, heating via alpha particles becomes important only when the shock wave has a large radius and the matter has low entropies. The dynamics in 2D are more sensitive to the inclusion of the light-nuclei heating because the SASI in the non-linear regime makes the gain region more inhomogeneous. In this inhomogeneity, regions appear that have densities and temperatures favorable for the existence of light nuclei. The heating rates of light nuclei reach about 10% of those of nucleons locally. As a consequence, the dynamics of shock revival are influenced by heating via light nuclei. In particular, heating by deuterons brings non-negligible changes, which may be positive or negative for shock revival, when the neutrino luminosity is close to the critical value. The results are rather sensitive to the neutrino spectrum. In the case of $T_{\nu_\mu} = 5$ MeV instead of $T_{\nu_\mu} = 10$ MeV, the heating of alpha particles is reduced by ~90% whereas heating via deuterons is not so much affected, since the CC reactions with ν_e and $\bar{\nu}_e$ are more important for the deuteron heating.

The numerical simulations in this paper are admittedly of an experimental nature and the numbers we have obtained may be subject to changes in more realistic simulations. We need more systematic investigations, varying not only the neutrino luminosity and mass accretion rate but also the neutrino

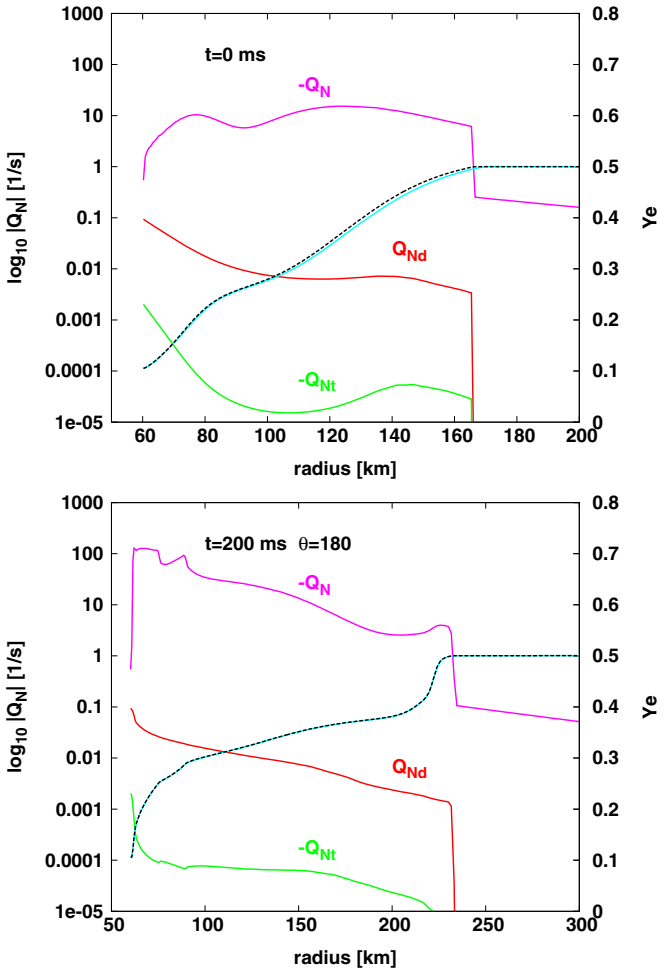

Figure 13. Electron fractions (black dotted line) and the absolute values of Q_N (magenta lines), Q_{Nd} (red solid lines), and Q_{Nt} (green solid lines) at $t = 0$ and 200 ms along the radial ray with $\theta = 180°$. See the text for the definitions of Q_N, Q_{Nd}, and Q_{Nd}. The electron fractions obtained with $Q_{Nd} = Q_{Nt} = 0$ are also shown by the cyan solid lines.

(A color version of this figure is available in the online journal.)

temperature, mass of the central object, and initial perturbations. The cooling reactions of light nuclei such as $d + e^- \rightarrow n + n + \nu_e$ and $n + p \rightarrow d + \nu + \bar{\nu}$ should be incorporated into the calculations, since deuterons are abundant in the cooling regions as shown in Figures 2 and 9. Recently, Nasu et al. (2013) demonstrated that the existence of deuterons reduces neutrino emissions by electron- and positron capture, since the capture rate of deuterons is lower than that of nucleons. Nasu et al. (2013) compared the total $e^{\pm}$-capture rates between models with and without deuterons at 150 ms after core bounce, employing the compositions of light nuclei as calculated in Sumiyoshi & Röpke (2008). Figures 1 and 2 in Nasu et al. (2013) indicate that this effect becomes remarkable inside the neutrino sphere but the reduction factor goes down below a few percent near the gain radius ($r \sim 90$ km). Note that this effect is included in our models except for the $e^{\pm}$-captures on deuterons. Although the latter rates are not available to us at the present, their contributions to the cooling would be less than a few percent of the cooling rates of nucleons in the gain region and the discussion in this article would not be changed significantly. Of course, the reactions will become important at the bottom of the cooling region. The neutrino transport should be improved so that the neutrino emission from accreting matter can be properly treated. For more realistic simulations, the central part of the core should also be solved self consistently. Last, but not least, the difference between 2D and 3D simulations should be made more clear. These issues are currently being tackled and will be reported elsewhere.

S.F. thanks T. Sato, S. Nasu, T. Fischer, W. I. Nakano, and Y. Yamamoto for their useful discussions. S.F. is supported by the Japan Society for the Promotion of Science Research Fellowship for Young Scientists. This work is partially supported by the Grant-in-Aid for Scientific Research on Innovative Areas (Nos. 20105004, 20105005), the Grant-in-Aid for the Scientific Research (Nos. 22540296, 24103006, 24244036, 24740165), and the HPCI Strategic Program and Excellent Graduate Schools from the Ministry of Education, Culture, Sports, Science, and Technology (MEXT). A part of the numerical calculations were carried out on SR16000 at YITP at Kyoto University.

REFERENCES

Arcones, A., Martínez-Pinedo, G., O'Connor, E., et al. 2008, PhRvC, 78, 015806
Barnea, N., & Gazit, D. 2008, FBS, 43, 5
Blinnikov, S. I., Panov, I. V., Rudzsky, M. A., & Sumiyoshi, K. 2011, A&A, 535, A37
Blondin, J. M., Mezzacappa, A., & DeMarino, C. 2003, ApJ, 584, 971
Botvina, A. S., & Mishustin, I. N. 2004, PhLB, 584, 233
Botvina, A. S., & Mishustin, I. N. 2010, NuPhA, 843, 98
Bruenn, S. W., Mezzacappa, A., Hix, W. R., et al. 2013, ApJ, 767, 6
Buras, R., Janka, H.-Th., Rampp, M., & Kifonidis, K. 2006a, A&A, 457, 281
Buras, R., Rampp, M., Janka, H.-Th., & Kifonidis, K. 2006b, A&A, 447, 1049
Burrows, A. 2013, RvMP, 85, 245
Burrows, A., Hayes, J., & Fryxell, B. A. 1995, ApJ, 450, 830
Couch, S. M. 2013, ApJ, 765, 29
Fernández, R. 2010, ApJ, 725, 1563
Fernández, R., & Thompson, C. 2009a, ApJ, 697, 1827
Fernández, R., & Thompson, C. 2009b, ApJ, 703, 1464
Foglizzo, T., Galletti, P., Scheck, L., & Janka, H.-T. 2007, ApJ, 654, 1006
Foglizzo, T., Masset, F., Guilet, J., & Durand, G. 2012, PhRvL, 108, 051103
Foglizzo, T., Scheck, L., & Janka, H.-Th. 2006, ApJ, 652, 1436
Fryer, C. L. 2004, ApJL, 601, L175
Fryer, C. L., Holz, D. E., & Hughes, S. A. 2002, ApJ, 565, 430
Furusawa, S., Sumiyoshi, K., Yamada, S., & Suzuki, H. 2013, ApJ, 772, 95
Furusawa, S., Yamada, S., Sumiyoshi, K., & Suzuki, H. 2011, ApJ, 738, 178
Gazit, D., & Barnea, N. 2004, PhRvC, 70, 8801
Hanke, F., Marek, A., Mueller, B., & Janka, H.-T. 2012, ApJ, 755, 138
Hanke, F., Marek, A., Müller, B., & Janka, H.-T. 2013, ApJ, 770, 66
Haxton, W. C. 1988, PhRvL, 60, 1999
Hempel, M., Fischer, T., Schaffner-Bielich, J., & Liebendörfer, M. 2012, ApJ, 748, 70
Hempel, M., & Schaffner-Bielich, J. 2010, NuPhA, 837, 210
Herant, M., Benz, W., & Colgate, S. 1992, ApJ, 395, 642
Iwakami, W., Kotake, K., Ohnishi, N., Yamada, S., & Sawada, K. 2008, ApJ, 678, 1207
Iwakami, W., Kotake, K., Ohnishi, N., Yamada, S., & Sawada, K. 2009, ApJ, 700, 232
Janka, H.-T. 2012, ARNPS, 62, 407
Kotake, K., Sato, K., & Takahashi, K. 2006, RPPh, 69, 971
Kuroda, T., Kotake, K., & Takiwaki, T. 2012, ApJ, 755, 11
Langanke, K., Martinez-Pinedo, G., Muüller, B., et al. 2008, PhRvL, 100, 011101
Lattimer, J. M., & Swesty, F. D. 1991, NuPhA, 535, 331
Marek, A., & Janka, H.-Th. 2009, ApJ, 694, 664
Marek, A., Janka, H.-T., & Müller, E. 2009, A&A, 496, 475
Müller, B., Janka, H.-T., & Heger, A. 2012, ApJ, 761, 72
Murphy, J. W., Dolence, J. C., & Burrows, A. 2013, ApJ, 771, 52
Nagakura, H., Ito, H., Kiuchi, K., & Yamada, S. 2011, ApJ, 731, 80
Nagakura, H., & Yamada, S. 2008, ApJ, 689, 391
Nagakura, H., Yamamoto, Y., & Yamada, S. 2013, ApJ, 765, 123
Nakamura, K., Takiwaki, T., Kotake, K., & Nishimura, N. 2013, ApJ, submitted (arXiv:1207.5955)
Nakamura, S. X., Sumiyoshi, K., & Sato, T. 2009, PhRvC, 80, 035802
Nasu, S., Sato, T., Nakamura, S. X., et al. 2013, FBS, 54, 1595

O'Connor, E., Gazit, D., Horowitz, C. J., Schwenk, A., & Barnea, N. 2007, PhRvC, 75, 055803
Ohnishi, N., Kotake, K., & Yamada, S. 2006, ApJ, 641, 1018
Ohnishi, N., Kotake, K., & Yamada, S. 2007, ApJ, 667, 375
Ott, C. D., Abdikamalov, E., Mösta, P., et al. 2013, ApJ, 768, 1150
Scheck, L., Kifonidis, K., Janka, H., & Müller, E. 2006, A&A, 457, 963
Scheck, L., Plewa, T., Janka, H.-T., Kifonidis, K., & Müller, E. 2004, PhRvL, 92, 011103
Shen, G., Horowitz, C. J., & Teige, S. 2011a, PhRvC, 83, 035802
Shen, H., Toki, H., Oyamatsu, K., & Sumiyoshi, K. 1998a, NuPhA, 637, 435
Shen, H., Toki, H., Oyamatsu, K., & Sumiyoshi, K. 1998b, PThPh, 100, 1013
Shen, H., Toki, H., Oyamatsu, K., & Sumiyoshi, K. 2011b, ApJS, 197, 20
Sumiyoshi, K., & Röpke, G. 2008, PhRvC, 77, 055804
Sumiyoshi, K., Yamada, S., Suzuki, H., et al. 2005, ApJ, 629, 922
Suwa, Y., Kotake, K., Takiwaki, T., Liebendörfer, M., & Sato, K. 2011, ApJ, 738, 165
Suwa, Y., Kotake, K., Takiwaki, T., et al. 2010, PASJ, 62, L49
Suwa, Y., Takiwaki, T., Kotake, K., et al. 2013, ApJ, 764, 99
Takiwaki, T., Kotake, K., & Suwa, Y. 2012, ApJ, 749, 98
Yamamoto, Y., Fujimoto, S., Nagakura, H., & Yamada, S. 2013, ApJ, 771, 27
Yamasaki, T., & Yamada, S. 2005, ApJ, 623, 1000